Transversal Patterns in Three-Dimensional Packed Bed Reactors: Oscillatory Kinetics

Olga Nekhamkina and Moshe Sheintuch
Dept. of Chemical Engineering, Technion - I.I.T., Technion City, Haifa 32 000, Israel

DOI 10.1002/aic.12199
Published online March 18, 2010 in Wiley Online Library (wileyonlinelibrary.com).

Formation of transversal patterns in a 3D cylindrical reactor is studied with a catalytic reactor model in which an exothermic first-order reaction of Arrhenius kinetics occurs with a variable catalytic activity. Under these oscillatory kinetics, the system exhibits a planar front (1D) solution with the front position oscillating in the axial direction. Three types of patterns were simulated in the 3D system: rotating fronts, oscillating fronts with superimposed transversal (nonrotating) oscillations, and mixed rotating–oscillating fronts. These solutions coexist with the planar front solution and require special initial conditions. We map bifurcation diagrams showing domains of different modes using the reactor radius as a bifurcation parameter. The possible reduction of the 3D model to the 2D cylindrical shell model is discussed. © 2010 American Institute of Chemical Engineers *AIChE J,* 56: 2887–2897, 2010
Keywords: reactor analysis, simulation, process, fronts, bifurcations, transversal patterns

Introduction

Heterogeneous catalytic PBRs are extensively used in chemical and petrochemical industry and for reduction of environmental pollution generated by automobiles, electrical power stations, and other processes. Oscillatory kinetics is typical for the oxidation of carbon monoxide, hydrogen, ammonia, hydrocarbons, alcohols, ethers, and formic acids as well as during nitrogen monoxide reduction by ammonia or carbon monoxide and the hydrogeneration of carbon monoxide or ethylene. The PBRs are known to exhibit stationary or moving thermal fronts propagating in the axial direction, in the case of sufficiently exothermic reactions (e.g., oxidation and hydrogenation) and oscillatory fronts in the case of oscillatory kinetics. The cross section temperature (and conversion) distributions, which are assumed to be uniform in an adiabatic PBR, may undergo symmetry breaking in the transversal (normal to the flow) direction under certain conditions. Several experimental studies reported formation of the hot spots in PBRs.[1–5] Obviously, tracking such symmetry breaking is difficult in large commercial reactors. Infrared imaging revealed temperature pattern formation in various laboratory reactors including the exterior surface of a radial flow reactor[6] and the top of shallow packed-bed reactors[7] or the surface of a catalytic cloth[8] under oscillatory conditions.

Significant modeling efforts have been directed to predict the formation of transversal patterns during the last decade (see a recently published review[9]). The analysis of a three-dimensional, two-phase reactor model, with complex kinetics is very intricate. Thus, previous studies have been conducted with simplified models which are derived from a general model using several assumptions concerning either the physical and kinetics models or geometrical symmetry assumed. The main and most popular physical reduction is that of using of a single-phase pseudo-homogeneous model,[10] which is justified in many processes (under certain conditions a heterogeneous model can be reduced to a pseudo-homogeneous one using effective mixing or dispersion coefficients that account for the interphase transport parameters).

The generic kinetic model used to study instability in PBRs accounts for a single exothermic reaction with Arrhenius kinetics and is described by two state variables: the temperature (T) and the concentration of a limiting species (C). For a 1D system such kinetics predicts, within

Correspondence concerning this article should be addressed to O. Nekhamkina at aermwon@tx.technion.ac.il.

appropriate domains of parameters, either a stable reaction front propagating with a constant form and a constant velocity (i.e., "frozen" in a moving coordinate) or an unstable "galloping" front.[11] The minimalistic model that accounts for an oscillatory behavior can be constructed by coupling such a two-variable (C–T) model with a third variable that describes a reversible change of a catalytic activity (θ) assuming that deactivation (activation) occurs at higher (lower) temperatures.

Several simplified 2D geometries have been proposed to facilitate the analysis of the full 3D system:
-A thin annular cylindrical shell reactor defined in the axial-azimuthal ($z - \phi$) plane.[12]
-A 2D model that ignores the azimuthal dependence operating in the axial-radial ($z - r$) plane.[13]
-A short monolith (SM)[14] or shallow reactor (SR) models[15,16] defined in the radial-azimuthal ($r - \phi$) plane. [SR models can be obtained using the Liapunov-Schmit reduction for a case of small axial gradients if we average the state variables in this direction while accounting for BC]. These are essentially reaction-diffusion (RD) systems, which are amenable to linear stability analysis.

The models of the first two simplified-geometry groups listed above may admit front solutions propagating in the axial direction. The planar front stability analysis with respect to transversal perturbations is a rather complex problem as the basic 1D front solution is not known analytically. Moreover, for the Arrhenius kinetics even the space-dependent steady states (fixed points of the source function) cannot be expressed analytically. We review certain results concerning fronts of the thermo-kinetic model, which are relevant to our study of oscillatory fronts: The maximal temperature rise over the front ($\Delta T_{\rm mx} = T_{\rm mx} - T_{\rm in}$) is related to the front velocity ($V_{\rm f}$) like[17]:

$$\Delta T_{\rm mx} = \Delta T_{\rm ad}\frac{1 - V_{\rm f}}{1 - LeV_{\rm f}}$$

where $\Delta T_{\rm ad}$ is the adiabatic temperature rise, Le is the Lewis number (the dimensionless heat capacity, see below). Approximate relations for $T_{\rm mx}$ and $V_{\rm f}$ are available for the limiting case $Pe_C \to \infty$ (Pe_C is the mass Peclet number)[18] and were recently extended by us for the case of finite Pe_C.[19] For this case, we have showed[20] that a planar front may bifurcate into nonrotating transversal patterns when

$$Pe_C/Pe_T < (1 - V_{\rm f})/(1 - LeV_{\rm f}) \qquad (1)$$

where Pe_T is the heat Peclet number. This novel condition can be satisfied for realistic systems (i.e. one with $Pe_C/Pe_T > 1$) only for an upstream propagating front. Criterion (1) was verified by direct numerical simulations of a 2D thin cylindrical shell model[12] showing formation of stable nonrotating transversal patterns on a shell of a sufficiently large diameter and transient structures with small D. Condition (1) predicts the emergence of patterns for stationary fronts when $Pe_C < Pe_T$. This is also the condition derived with the SR model for both the pseudo-homogeneous[15] and for the two-phase heterogeneous models.[21] This is exactly a condition of the Turing mechanism.

Similar conditions were derived for two-variable activator-inhibitor RD systems with polynomial kinetics: the planar front was shown to be unstable with respect to transversal perturbations if the ratio of the diffusion coefficient for the activator to that for inhibitor exceeds some critical value.[22,23] The basic characteristic of transversal patterns beyond the bifurcation condition can be determined by dispersion curves showing dependence of the temporally perturbation growth as functions of a wave number, which were conducted with a cubic kinetics by several groups.[24–26]

For oscillatory kinetics, any analytical results concerning the planar (1D) front parameters and their stability, to the best of our knowledge, were not published yet. That makes the stability analysis a numerical problem. Numerical stability analysis is briefly described in Appendix since it will be useful to explain some of our results. Such analysis considers transversal perturbations of the form of transversal eigenfunctions:

$$F_{\perp}(r,\phi) = J_m(\mu_{mn}r)\exp(im\phi) \qquad (2)$$

where the radial eigenfunctions $J_m(\mu_{\rm mn}r)$ are the Bessel functions of the first kind, $\mu_{\rm mn}$ are the transversal eigenvalues.

Previous studies were focused on linear analysis of the first four modes (see Figure 1 with the corresponding $\mu_{\rm mn}$) in either 3D[16,27,28] or shallow reactor models[15,16,29,30] and did not simulate patterns. Linear analysis suggests formation of moving nonrotating patterns of the form (2) while the unstable domains of certain modes were quite similar in 3D and SR models. Any critical conditions on the diffusivities of the state variables was not revealed.

Direct numerical simulations using the full 3D model are very tedious and were not reported yet. The available results obtained for oscillatory kinetics with simplified 2D models show:
-With the cylindrical shell model and the three-variable (C–T–θ) kinetics two types of solutions were revealed with $Pe_C \gg Pe_T$[12]: (i) oscillating fronts with superimposed nonrotating

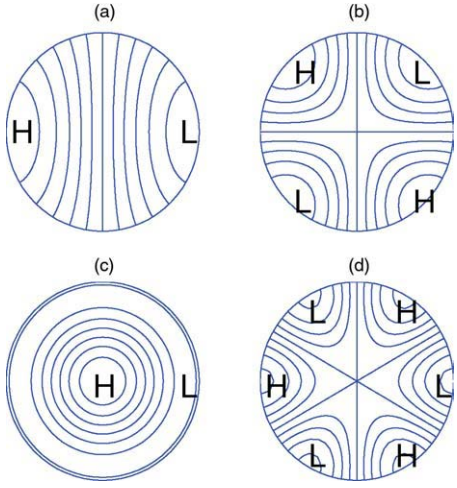

Figure 1. Schematic diagrams of the first four transversal eigenfunctions $J_m(\mu_{\rm mn}r)$ exp ($im\phi$) defined by Eq. 2.

$\mu_{11} = 1.84$ (1), $\mu_{21} = 3.0542$ (2), $\mu_{01} = 3.83$, (3) and $\mu_{31} = 4.20$ (4). [Color figure can be viewed in the online issue, which is available at wileyonlinelibrary.com.]

patterns and (ii) rigid rotating fronts with one wave or multiple waves.

-With the 2D azimuthally symmetric model complex transversal patterns including period-doubling oscillations were obtained.[13]

-With the SR model moving nonrotating patterns of the form (2) were obtained for different oscillatory kinetics. The complexity of patterns increased with R.[30]

At the same time, RD systems with oscillatory or excitable kinetics are known to exhibit moving targets and rotating spirals[31–34] in sufficiently large 2D domains rather then patterns of the form (2). In 3D RD systems, a homogeneous steady state can bifurcate into a scroll wave vortex rotating around a filament similarly to a rotating spiral wave in a 2D case.[35,36] Such patterns cannot be predicted by linear stability analysis using modes (2), but can be analyzed using a kinematic approach.[34] Note that on a disk of finite R coexistence of rotating spirals with a new type of patterns in the form of spots moving along the disk boundary was detected recently.[37]

The question we pose is, what types of transversal patterns can be sustained in 3D cylindrical RDA systems? In the present work, we analyze pattern selection in 3D PBRs with oscillatory kinetics using a three-variable (C–T–θ) model under conditions when a planar front solution exhibits an axial oscillatory front behavior. An analytical study is extremely complicated in such a case (see discussion above) and we focus on direct numerical simulations of 3D PBRs using various initial conditions and trace the sustained patterns with varying the reactor radius.

The structure of this study is as follows: after presenting the model and its 1D (axial) solution, in the third section, we present and classify the simulated transversal patterns. In concluding remarks, we discuss the results and also address the possible reduction of the 3D model results to 2D cases.

Reactor Model

We analyze pattern formation for the generic pseudo-homogeneous model of a fixed bed reactor catalyzing a first-order exothermic reaction with Arrhenius kinetics. In the adiabatic case, assuming noncatalytic reactor walls, the balance equations may be written in the following dimensionless form:

$$\frac{\partial x}{\partial \tau}+\frac{\partial x}{\partial \xi}-\frac{1}{Pe_C}\frac{\partial^2 x}{\partial \xi^2}-\frac{1}{Pe_C \bar{R}^2}\left[\frac{1}{\bar{r}}\frac{\partial}{\partial \bar{r}}\left(\bar{r}\frac{\partial x}{\partial \bar{r}}\right)+\frac{1}{\bar{r}^2}\frac{\partial^2 x}{\partial \phi^2}\right]=f(x,y,\theta) \quad (3)$$

$$Le\frac{\partial y}{\partial \tau}+\frac{\partial y}{\partial \xi}-\frac{1}{Pe_T}\frac{\partial^2 y}{\partial \xi^2}-\frac{1}{Pe_T \bar{R}^2}\left[\frac{1}{\bar{r}}\frac{\partial}{\partial \bar{r}}\left(\bar{r}\frac{\partial y}{\partial \bar{r}}\right)+\frac{1}{\bar{r}^2}\frac{\partial^2 y}{\partial \phi^2}\right]=Bf(x,y,\theta), \quad (4)$$

$$f(x,y,\theta)=Da\theta(1-x)\exp\left(\frac{\gamma y}{\gamma+y}\right), \quad (5)$$

The boundary conditions imposed are the traditional Danckwerts type:

$$\xi=0, \quad \frac{1}{Pe_C}\frac{\partial x}{\partial \xi}=x, \quad \frac{1}{Pe_T}\frac{\partial y}{\partial \xi}=y,$$

$$\xi=1, \quad \frac{\partial x}{\partial \xi}=0, \quad \frac{\partial y}{\partial \xi}=0. \quad (6)$$

$$\bar{r}=1, \ \ \partial x/\partial \bar{r}=0, \ \ \partial y/\partial \bar{r}=0$$

Here, x and y are conversion and the dimensionless temperature, respectively, θ is the catalytic activity, Da, Le, Pe_T, and Pe_C are the dimensionless reaction velocity (Damkohler), heat capacity (Lewis), and dispersivities of heat and mass (Peclet numbers), respectively, B is the dimensionless exothermicity. All parameters are conventionally defined:

$$x=1-\frac{C}{C_{\text{in}}},\ y=\gamma\frac{T-T_{\text{in}}}{T_{\text{in}}},\ \xi=\frac{z}{L},\ \bar{r}=\frac{r}{r_{\text{w}}},\ \tau=\frac{tu}{L},\ \bar{R}=\frac{r_{\text{w}}}{L},$$

$$\gamma=\frac{E}{RT_{\text{in}}},\ \Delta T_{\text{ad}}=\frac{(-\Delta H)C_{\text{in}}}{(\rho C_p)_{\text{f}}},\ B=\gamma\frac{\Delta T_{\text{ad}}}{T_{\text{in}}},$$

$$Da=\frac{L}{u}A\exp(-\gamma),\ Le=\frac{(\rho c_p)_{\text{e}}}{(\rho c_p)_{\text{f}}},$$

$$Pe_T=\frac{(\rho c_p)_{\text{f}}Lu}{k_{\text{e}}},\ Pe_C=\frac{Lu}{\varepsilon D_{\text{f}}}$$

In the following text, bars over r and R will be omitted.

The system above with $\theta = 1$ may admit moving (or stationary) front solutions.[38] To admit an oscillatory behavior, we vary the catalytic activity using a simple linear expression[12,39] that assumes that deactivation occurs faster at higher temperatures and at higher activities and that its rate is independent of the reactant concentration. The dimensionless form of the catalytic activity variation is:

$$K_\theta\frac{d\theta}{d\tau}=a_\theta-b_\theta\theta-y \quad (7)$$

Numerical methods

Numerical simulations were conducted using an implicit finite-difference scheme based on approximate factorization. The 1D simulations were conducted using a grid composed of equally spaced 513_z points. The 3D simulations were conducted using a grid with $513_z \times 65_\phi \times 41_r$ points with the time step $\Delta\tau = 0.001 - 0.02$. Several control runs were conducted on a finer (in the transversal direction) grid with $513_z \times 129_\phi \times 81_r$ points.

Planar front characteristics

We used a certain set of parameters (see Figure 2) for which the 1D system [Eqs. 3–7 with omitted transversal gradients] exhibits a front solution that oscillates in the axial direction. This behavior emerges over a wide domain. This set was also used in our previous study of pattern formation in a 2D cylindrical shell model.[12]

For the chosen set of parameters, the 1D front position (Z_{f}), defined as the z-position corresponding to a fixed conversion ($x = 0.5$), oscillates between $Z_{\text{f}} = 0.684 - 0.8144$ (Figure 2a). The front velocity (V_{f}) exhibits relaxation oscillations with sharp changes in values followed by gradual

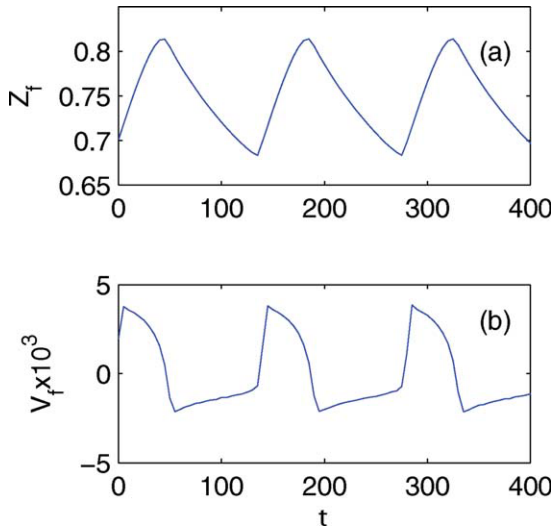

Figure 2. Typical 1D oscillatory planar front solution of system (3–7) showing the temporal behavior of the front position (Z_f, a) and of the front velocity (V_f, b).

$Da = 0.06$, $B = 30$, $\gamma = 20$, $Le = 100$, $Pe_T = 500$, $Pe_C = 5000$, $K_\theta = 66.7$; $a_\theta = 26.7$, $b_\theta = 33.3$. [Color figure can be viewed in the online issue, which is available at wileyonlinelibrary.com.]

change (Figure 2b). The period of axial oscillations is $P_{ax} = 140.5$ with duration of the downstream and the upstream propagation parts approximately related as 1:2.

3D PBR Simulations

Three types of transversal patterns were detected: rotating fronts, transversally-inhomogeneous fronts oscillating in the axial direction, and mixed rotating–oscillating motion. These exist in certain domains described below and coexist (at least, for the case of small R) with a transversally-homogeneous oscillating front. To obtain the patterned states, we used as IC a certain 1D profile slightly perturbed in the transversal plane in the vicinity of the front position (the choice of IC is discussed in the last section of the article). Once the transversely inhomogeneous solution was obtained, it was traced by decreasing/increasing R to construct the bifurcation diagrams.

To describe the sustained structures, we calculated the front position Z_f (r, ϕ, τ) for each point in the transversal plane (r, ϕ) as a function of time. Using this 2D field distribution, we defined:

(i) Local maximal [Z_f^{mx} (τ)], minimal [Z_f^{mn} (τ)], and averaged [Z_f^{av} (τ)] front positions:

$$Z_f^{mx}(\tau) = \max_{r,\phi}\{Z_f(r,\phi,\tau)\},$$
$$Z_f^{mn}(\tau) = \min_{r,\phi}\{Z_f(r,\phi,\tau)\},\ Z_f^{av}(\tau) = \langle\langle Z_f(r,\phi,\tau)\rangle\rangle_{\phi,r}$$

(ii) The maximal [$\Delta Z_\perp$ (τ)] and the time averaged [$\Delta Z_\perp^{av}$] transversal front divergence:

$$\Delta Z_\perp(\tau) = Z_f^{mx}(\tau) - Z_f^{mn}(\tau),\ \Delta Z_\perp^{av} = \langle \Delta Z_\perp(\tau)\rangle_\tau$$

(iii) For rotating patterns – a local tip position in the transversal plane (r_{tip}, ϕ_{tip}) is defined (following Ref. 30) at each cross-section (ξ = const) as the point where the cross product between the gradient vectors of the two leading state variables y and x is maximal:

$$(\nabla y \times \nabla x)_{r_{tip},\phi_{tip}} = \sup\{(\nabla y \times \nabla x)_{r,\phi}, \forall r, \phi\} \qquad (8)$$

The locus of tips points forms a filament in the axial direction varying with time.

Rotating and mixed rotating–oscillating fronts

Pattern classification can be conducted following the filament motion (Figure 3) and in a simplified way following the tip location traced in the transversal plane with fixed axial position around the averaged front position (Figure 4). Rigid rotating fronts appear as a quasi-linear filaments, which are "frozen" in a rotating frame (Figure 3a) and

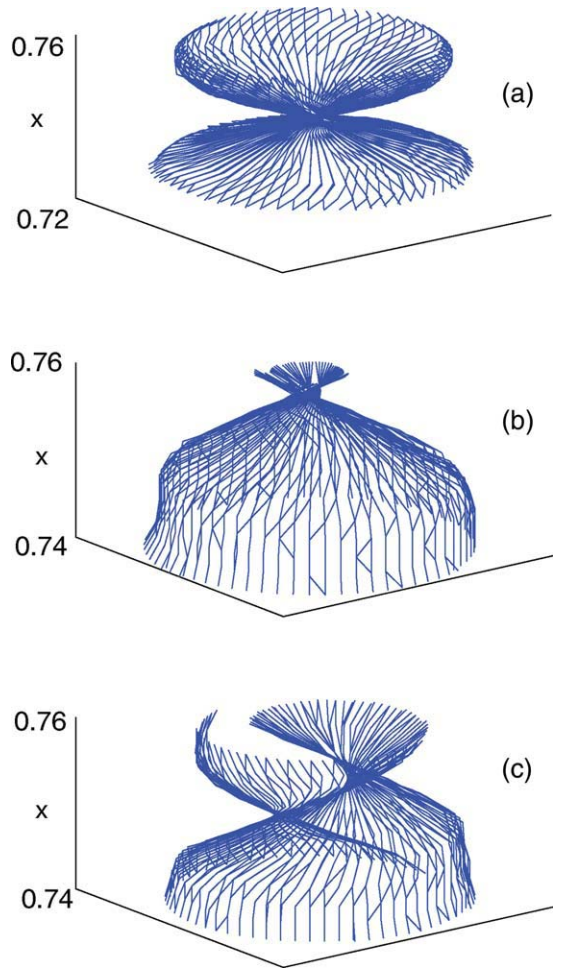

Figure 3. The spatial filament motion for typical rotating (a, R = 0.03) and mixed rotating–oscillating patterns (b, c, R = 0.023).

Plate a presents one rotation where the filament connecting the tip points completes one revolution. Plates b and c show time intervals corresponding to the front position around its downstream direction-reversal point and in the middle part of the reactor, respectively. Other parameters as in Figure 2. [Color figure can be viewed in the online issue, which is available at wileyonlinelibrary.com.]

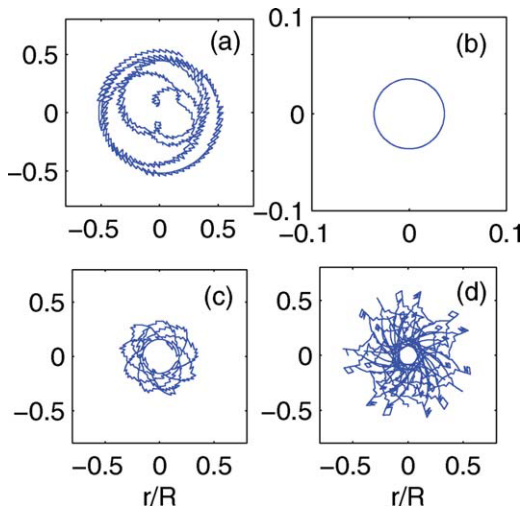

Figure 4. The tip motion in a cross-section corresponding to the average axial front position showing distinction between mixed rotating–oscillating (a,c,d) and rigid rotating (b) patterns.

$R = 0.023$ (a), 0.035 (b), 0.045 (c), and 0.06 (d). Other parameters as in Figure 2. [Color figure can be viewed in the online issue, which is available at wileyonlinelibrary.com.]

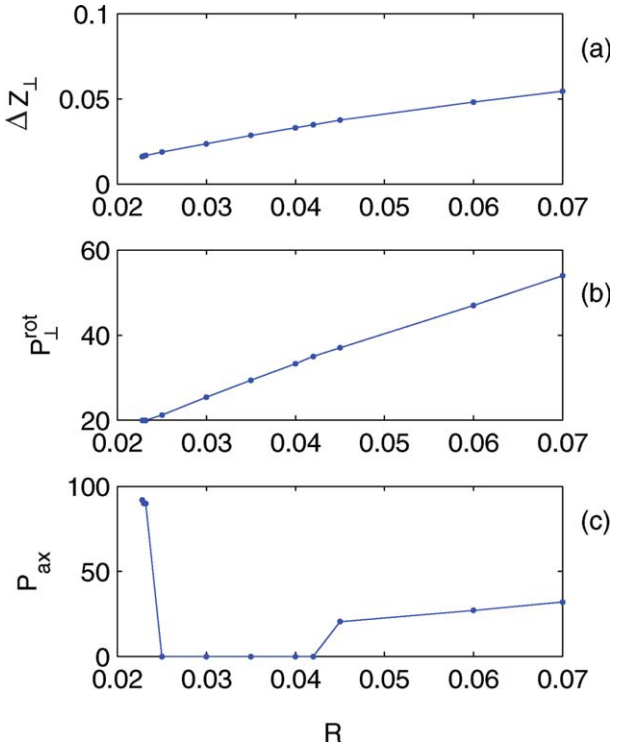

Figure 5. Bifurcation diagrams for rotating and mixed rotating–oscillating fronts showing the transversal front divergence ($\Delta Z_\perp$, a) and the period of transversal ($P_\perp^{rot}$, b), or axial (P_{ax}, c) oscillations vs. the reactor radius R.

Parameters as in Figure 2. [Color figure can be viewed in the online issue, which is available at wileyonlinelibrary.com.]

exhibit simple circles in transversal cross-sections (Figure 4b). The front rotates as a rigid object with a small hot spot upstream of the front and a large one downstream, with opposite ϕ-positions of the tips.

Mixed rotating–oscillating patterns appear as scrolled filaments and their rotation is superimposed on the axial front oscillations. To elucidate this behavior, we plotted the filaments for two time intervals corresponding to the front position around its downstream direction-reversal point (Figure 3b) and in the middle part of the reactor (Figure 3c). In transversal cross-sections, the tips exhibit complex meandering motion (Figures 4a, c, d).

Three domains of the system behavior are presented in Figure 5 showing the time-averaged transversal front divergence ($\Delta Z_\perp^{av}$, a), the period of rotation ($P_\perp^{rot}$, b) and of axial oscillations (P_{ax}, c) as functions of the reactor radius R: In the middle, rigid rotation domain ($R \simeq 0.0232-0.04$), $P_{ax} = 0$, whereas on the left and on the right domains $P_{ax} \neq 0$ and quasi-periodic mixed oscillations appear due to coexistence of (at least) two incommensurate frequencies corresponding to the axial and transversal oscillations. The low-R domain exists for $R \simeq 0.0228-0.0232$. We were not able to identify the bifurcation point from the transversally homogeneous solution. The right domain of mixed rotating–oscillating fronts exists for $R \simeq 0.4-0.7$. The corresponding tip motions exhibit meandering behavior as in a low-R domain (Figures 4c, d), which reflects the coexistence of several frequencies. We explain below the difference between these two quasi-periodic domains.

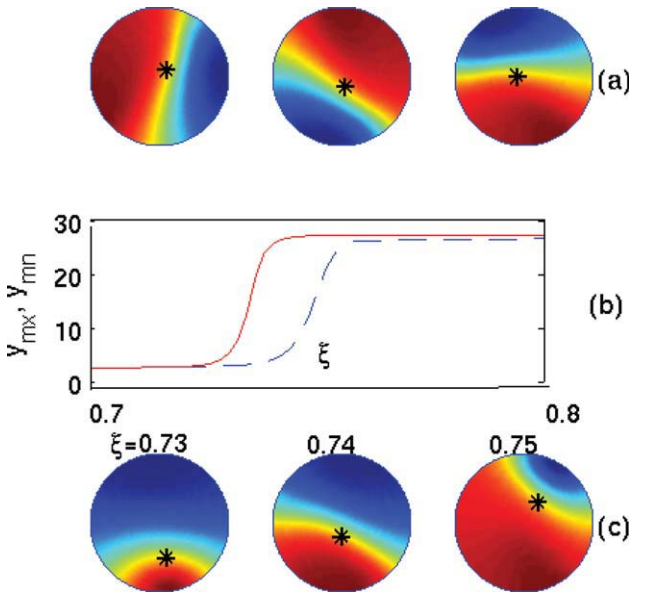

Figure 6. Typical mixed rotating–oscillating patterns in the low-R domain showing temporal (a) and spatial (b and c) transformations of the temperature field.

Several temperature snapshots in the cross-section at the average axial front position (a), axial profiles of the maximal (y_{mx}), and the minimal (y_{mn}) temperature (b, solid and dashed lines, respectively), and several snapshots along the reactor axis (c, numbers indicate the axial position). Stars mark the tip positions. $R = 0.023$, other parameters as in Figure 2. [Color figure can be viewed in the online issue, which is available at wileyonlinelibrary.com.]

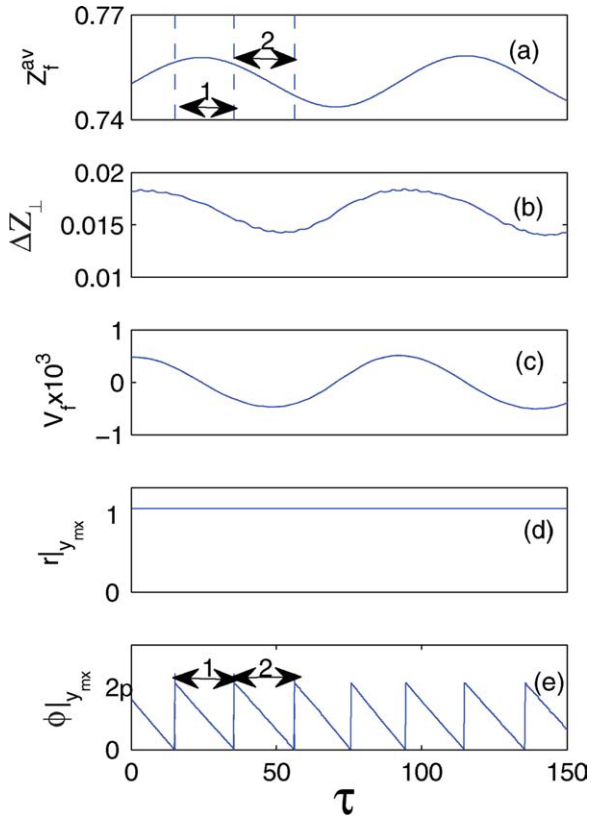

Figure 7. Typical mixed rotating–oscillating patterns in the low-*R* domain showing temporal behavior of the averaged front position (Z_f^{av}, a), the maximal transversal front divergence ($\Delta Z_\perp$, b), the average front velocity (V_f, c), the radial ($r|_{y_{mx}}$, d), and the angular ($\phi|_{y_{mx}}$, e) position of the maximal temperature y_{mx} at the front ($z = Z_f$).

Double arrows with numbers in (a and e) mark intervals corresponding to plates b and c of Figure 3. The parameters as in Figure 6. [Color figure can be viewed in the online issue, which is available at wileyonlinelibrary.com.]

Low-R domain. Typical temperature snapshots taken at a reactor cross-section moving with the average front position during one rotation (Figure 6a) show a high- and a low-temperature domains with extreme temperatures at the opposite disk edges and a clear rotating pattern. Typical axial profiles that describe the maximal (y_{mx}) and the minimal (y_{mn}) temperature distribution at a moment corresponding to the maximal transversal front divergence are shown in Figure 6b along with several cross-sections of the temperature field taken at a laboratory coordinate system (Figure 6c). As expected, the maximal transversal inhomogeneity takes place around the front position where the temperature difference is close to the maximal temperature rise over the front, y_m. The pattern transformation in the axial direction is as follows: a small domain of higher temperature emerges at the edge at a certain distance before the front and gradually expands downstream, finally conquering the whole reactor cross-section.

The temporal behavior of the averaged parameters is illustrated by Figure 7 showing the averaged front position (Z_f^{av}, a), the transversal front divergence ($\Delta Z_\perp$, b), the front velocity (V_f, c) along with the radial ($r|_{y_{mx}}$, d) and the angular ($\phi|_{y_{mx}}$, e) positions of the hot spot at the front.

The sustained pattern exhibits two different periods: one associated with axial oscillations is P_{ax} [$\simeq 90$ in case of Figures 7a–c], whereas the rotation period is $P_\perp^{rot}$ ($\simeq 19.5$ in case of Figure 7e). The transversal patterns are quasi-frozen and rotate with almost constant velocity. The ratio of these periods is $P_{ax}/P_\perp^{rot} > 1$. The averaged axial front oscillations (Figure 7a) occur around the average 1D front position ($\simeq 0.75$, see Figure 2a), but with significantly smaller amplitude than in the 1D case. The temporal Z_f^{av} (τ) dependence is almost harmonic in this case. The transversal front divergence ($\Delta Z_\perp$, Figure 7b) slightly varies with time and is synchronized with the axial motion: the divergence shrinks when the front approaches its direction-reversal points and increases during both the downstream and the upstream motion reaching its maximal value ($\simeq 0.018$) during the downstream phase.

High-R domain. Typical temperature snapshots of the reactor cross-section at the front position during three rotation periods are illustrated by Figure 8. Transversal structures essentially vary with time: hot spot can penetrate from the edge into the interior of the cross-section showing sharp changes of its radial position ($r|_{y_{mx}}$, Figure 9d) and of the pattern curvature, contrary to the low-*R* domain. Moreover, rotation occurs with a varying angular velocity (Figure 9e) and we did not find any regular regime within the whole domain of *R* that was studied.

"Non frozen" type of rotation is reflected by varying the transversally-averaged performance (which are constants for rigid rotation) and emergence of the averaged front position oscillations of period P_{ax} ($\simeq 27$ with $R = 0.06$, Figures 9a–

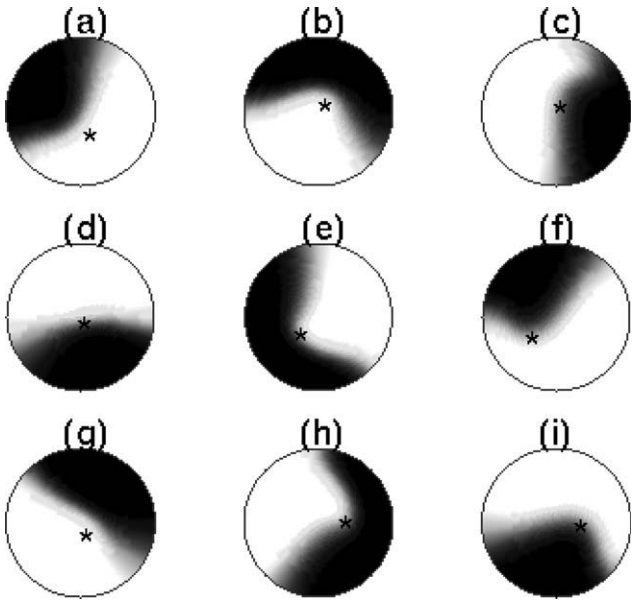

Figure 8. Typical mixed rotating–oscillating patterns in the large-*R* domain showing temporal transformation of the temperature snapshots in the cross-section at the average front position.

Stars mark the tip positions. $R = 0.06$, other parameters as in Figure 2.

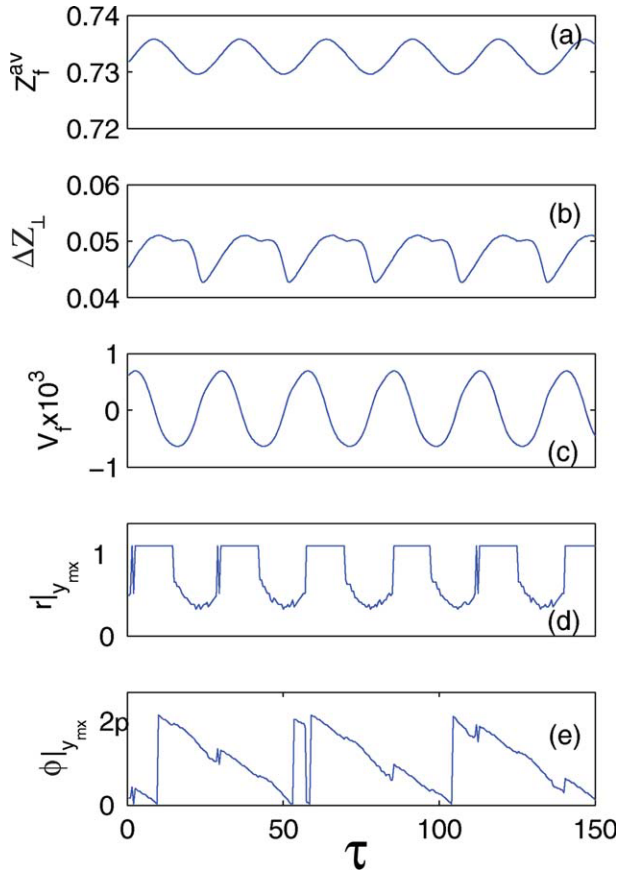

Figure 9. Mixed rotating–oscillating patterns in the large-*R* domain showing temporal behavior of the averaged front position (Z_f^{av}, a), the maximal transversal front divergence ($\Delta Z_\perp$, b), the average front velocity (V_f, c), the radial ($r|_{y_{mx}}$, d), and the angular ($\phi|_{y_{mx}}$, e) position of the maximal temperature y_{mx} at the front ($z = Z_f$).

Parameters as in Figure 8. [Color figure can be viewed in the online issue, which is available at wileyonlinelibrary.com.]

c). Coexistence of two oscillation processes leads to complex filament motion (Figure 3b) and meandering tip trajectories (Figures 4c, d).

The transversal front divergence (ΔZ_f, Figure 9b) increases with R as do the period of axial oscillations, which is still smaller then the period of rotation ($P_\perp^{rot} \simeq = 47$ in Figure 9e) contrary to the low-R domain where $P_{ax}/P_\perp^{rot} > 1$. The pattern transformation in the axial direction is quite similar to the low-R domain.

Note that increasing R leads to practically linear increase in the time-average transversal front divergence ($\Delta Z_\perp^{av}$) and of rotating period ($P_\perp^{rot}$) within all three domains shown in Figure 5. Continuation along this branch for sufficiently large R (>0.7, not shown) leads to complex rotation patterns with several distinct hot spots.

Oscillating transversally-inhomogeneous patterned fronts

Axially oscillating fronts with nonrotating transversal patterns that resemble the form of transversal eigenfunctions

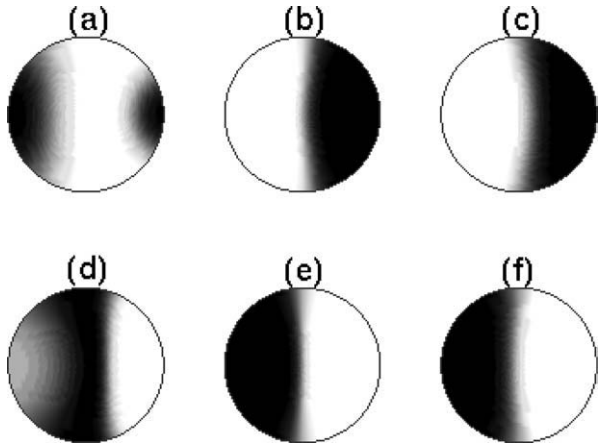

Figure 10. Typical Mode 1 oscillating front solutions showing several temperature snapshots in the cross-section at the average axial front position during the downstream (a–c) and the upstream (d–f) motion.

$R = 0.13$, other parameters as in Figure 2.

(Eq. 2, Figure 1), emerge if such functions are used as initial perturbations that are superimposed on the transversely homogeneous 1D solution. We consider below the oscillating fronts that resemble the first and the third modes (Figures 1a, c).

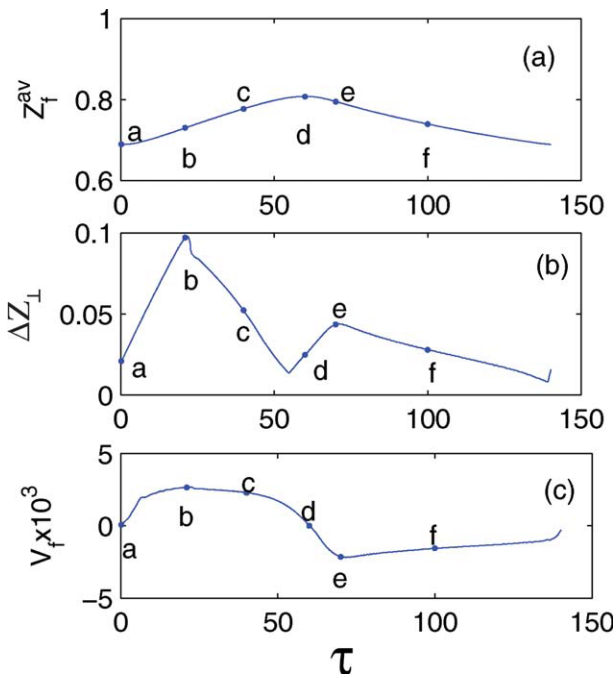

Figure 11. Typical Mode 1 oscillating front solution showing the temporal behavior of the average front positions [Z_f^{av}, a), the maximal transversal front divergence ($\Delta Z_\perp$, b), and the average front velocity (V_f, c).

Letters (a–f) mark moments corresponding to the snapshots shown in Figures 10a–f. Parameters as in Figure 10. [Color figure can be viewed in the online issue, which is available at wileyonlinelibrary.com.]

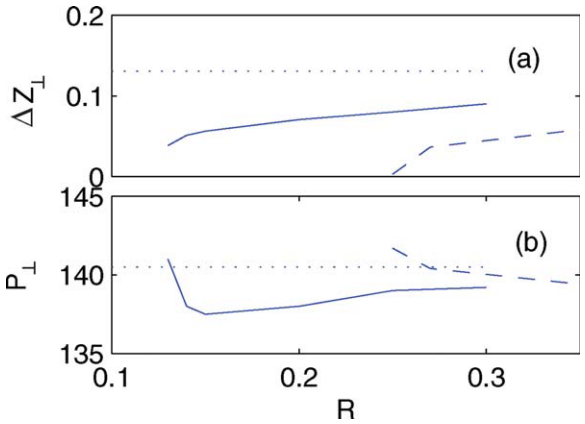

Figure 12. Bifurcation diagrams for oscillating front solutions showing the transversal front divergence ($\Delta Z_\perp$, a) and the period of axial ($P_\perp$, b) oscillations vs. the reactor radius R.

Solid and dashed lines mark the Mode 1 and the Mode 3 oscillating patterns, respectively. Dotted lines mark a 1D planar solution. Parameters as in Figure 2. [Color figure can be viewed in the online issue, which is available at wileyonlinelibrary.com.]

Mode 1 patterns: Sustained patterns of this kind show a high- and a low-temperature domains with a boundary between them that oscillates with time while preserving the symmetry of IC (snapshots of the reactor cross-section at the front position are shown in Figure 10). The corresponding temporal behavior of the averaged front positions (Z_f^{av}, a), the maximal transversal front divergence ($\Delta Z_\perp$, b) and the front velocity (V_f, c) are illustrated in Figure 11. The periods of transversal transformation and the axial oscillations are completely synchronized in a wide domain of R (0.13–0.3) starting from the bifurcation point $R = R_{3D}^{*1}$ ($\simeq 0.1253$ in our case, Figure 12).

The transversal front divergence [$\Delta Z_\perp$ (τ)] gradually enlarges and shrinks during the downstream and upstream sections of the front motion and reaches its minimum close to points of the front direction reversal (Figure 11, points a, d). At these points, the cold and the hot domains are interchanged forming antiphase oscillations (compare the upper and lower rows of Figure 10). The antiphase structure is clearly seen from the spatiotemporal pattern constructed using the temperature distribution along a horizontal diameter (the symmetry axis in this case) at the reactor cross-section following the averaged front position (Figure 13a). At the same time, the similar spatiotemporal pattern constructed for any fixed z-position (time averaged, $\langle Z_f^{av}(\tau)\rangle_\tau$, front position is shown in Figure 13b) is significantly smoother as it includes extended periods of quasi-homogeneous upper/lower solutions when the front leaves the corresponding cross-section.

Typical axial pattern transformation at a moment corresponding to the maximal transversal front divergence is illustrated in Figure 14 showing the maximal (y_{mx}) and minimal (y_{mn}) temperature profiles (row a) and temperature snapshots at several cross-sections (row b). Because of symmetry of the Mode 1 solution, y_{mx} (r, ϕ) and y_{mn} (r, ϕ) lie on the symmetry (horizontal in the case of Figsures 10 and 14) axis of each cross-section ξ = const. Along the axial direction, the maximal transversal inhomogeneity takes place around the front position where the temperature difference is close to the maximal temperature rise over the front, y_m, as in the case of rotating patterns. The pattern transformation in the axial direction is also similar: a hot spot emerges at the edge at a certain distance before the front and gradually expands downstream, finally conquering the whole reactor cross-section.

With increasing R, the averaged transversal front divergence ($\Delta Z_\perp^{av}$) gradually increases (Figure 12a) whereas the period of oscillations ($P_\perp$, Figure 12b) is practically independent on R and is close to that of the 1D homogeneous front oscillations.

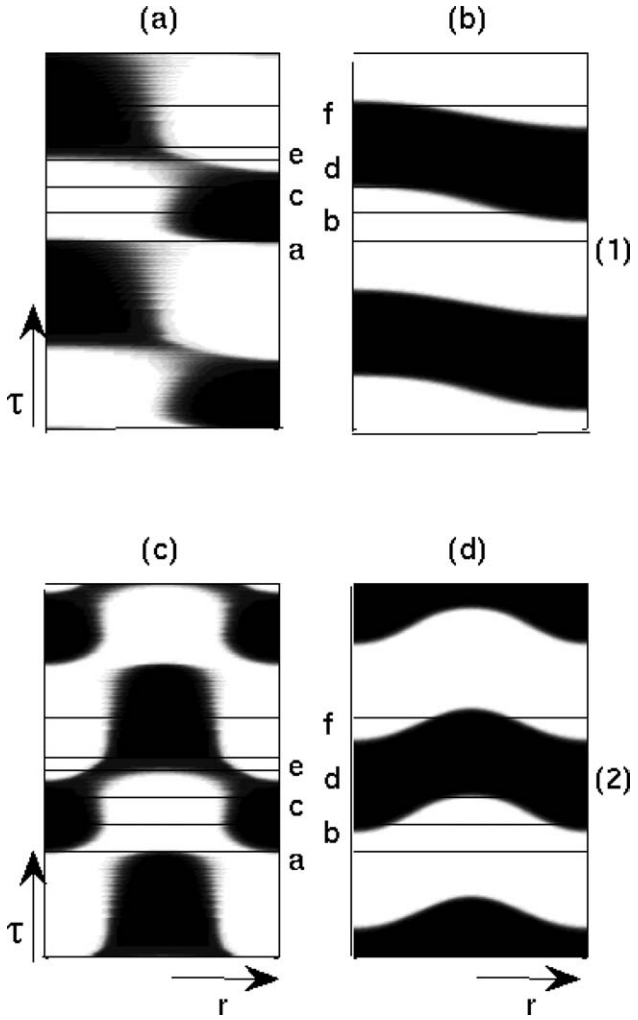

Figure 13. Typical oscillating front solution showing the Mode 1 (a & b) and the Mode 3 (c & d) spatio-temporal pattern constructed with the temperature profiles along the horizontal diameter in the cross-section moving with the front position, Z_f (τ) (a) and at the timely-averaged front position $\langle Z_f(\tau)\rangle$ (b).

Lines (a–f) in Row 1 mark moments corresponding to the snapshots shown Figure 10. Lines (a–f) in Row 2 mark moments corresponding to the snapshots shown in Figure 15 below $R = 0.13$ (a & b), 0.30 (c & d), other parameters as in Figure 2.

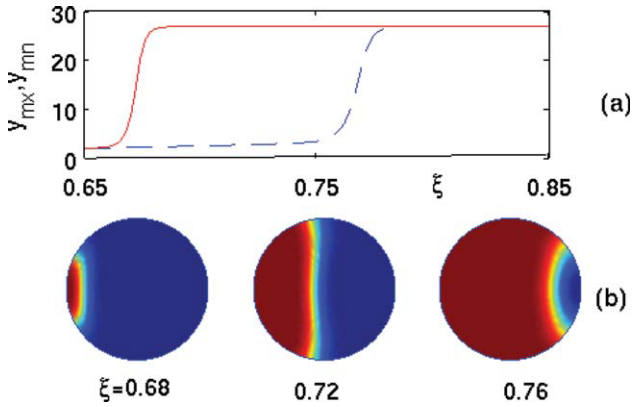

Figure 14. Typical axial transformation of the Mode 1 oscillating front solution showing the maximal (y_{mx}) and the minimal (y_{mn}) temperature profiles (a, solid and dashed lines, respectively) and several snapshots along the reactor axis (b).

Numbers in Row b indicate the axial position. Parameters as in Figure 10. [Color figure can be viewed in the online issue, which is available at wileyonlinelibrary.com.]

Evidently, due to the rotation symmetry, the system can exhibit infinitely many similar patterns shifted by an arbitrary azimuthal angle $\Delta\phi$.

Mode 3 patterns: The system behavior in this case is somewhat similar to the previous one: the transversal oscillations are completely synchronized with the axial front propagation yielding antiphase patterns at the points of front reversals: Although the downstream-moving front has a cold rim and a hot center, the upstream propagating front has a hot rim and a cold center (Figure 15, moving coordinates). Thus, the spatiotemporal pattern constructed using the temperature distribution along a certain diameter at the reactor cross-section following the averaged front position looks like a chess-board (Figure 13c), whereas the similar spatiotemporal pattern constructed for any fixed z-position [time averaged, $\langle Z_f^{av}(\tau)\rangle_\tau$, front position is shown in Figure 13d] is significantly smoother and exhibits an inward moving structure. Note that the Mode 3 spatio-temporal patterns (Figure 13, Row 2) looks like double Mode 1 patterns (Figure 13, Row 1) following the type of the corresponding eigenfunctions (2). With increasing R, a circular symmetry is destroyed leading to formation of transversal pattern of lower symmetry like those shown in Figure 15.

The branch of the Mode 3 oscillating front terminates upon decreasing R at critical $R = R_{3D}^{*3}$ ($\simeq$ 0.25 in our case, see Figure 12). The critical radii of the Mode 1 and the Mode 3 patterns are related approximately as 1:2, which is close to the ratio of the corresponding eigenvalues ($\mu_{11}/\mu_{01} \backsimeq 1.84{:}3.83$).

Discussion and Concluding Remarks

This is the first work to simulate three-dimensional spatiotemporal patterns in packed bed reactors or any RDA systems. It shows the emergence of rotating, oscillating, and mixed rotating–oscillating patterns in a PBR for certain oscillatory kinetics. Oscillations have been observed in many oxidation and hydrogenation catalytic reactions. Studies using a 2D version with axial symmetry[13] will not be able to reveal rotating patterns. This behavior is of academic and practical importance, as the PBR is the workhorse of the chemical-producing and pollutant abatement industry, and here we tried to address the academic interest. Of the practical implications we should point out just a few:

1 Transversal patterns can emerge with $Pe_C \gg Pe_T$ (even for $1/Pe_C = 0$), as was shown for other 2D versions with oscillatory kinetics.[12,29,30] This condition is valid in most systems. In contrast, transversal patterns in the regular thermo-kinetic model (i.e., $\theta = 1$) may emerge under condition (1), which applies only for an upstream propagating front.

2 Transversal patterns emerge for a reasonable radius/length ratio; they are more likely for larger R-values. A criterion for the minimal radius/length ratio (i.e., the wave length) is required for design purposes.

3 All transversal patterns coexist with the 1D oscillatory front solution; thus, if interested in a transversally-homogeneous solution one should design such a system with boundary-conditions (initial heating or cooling, and flow distribution) that should be as transversally homogeneous as possible. This requirement is more restrictive for large diameter reactors.

Other points to notice:

(i) The transversal patterns of oscillating fronts preserve the symmetry of IC if they resemble the form of transversal eigenfunctions. Simple rotating patterns are composed of low- and high-temperature domains separated by a curvilinear boundary.

(ii) The periods of transversal and axial oscillations of oscillating fronts are completely synchronized (at least at small R) and are close to that of the 1D motion. Rotating front solutions exhibit three subdomains: the system sustains

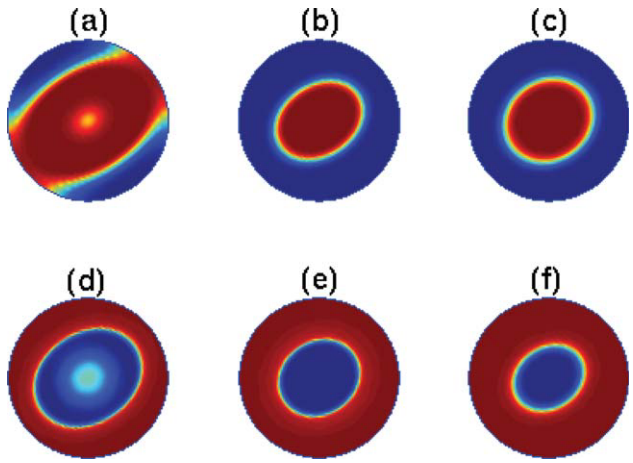

Figure 15. Typical Mode 3 oscillating front solution showing several temperature snapshots in the cross-section at the average axial front position during the downstream (a–c) and the upstream (d–f) motion.

$R = 0.3$, other parameters as in Figure 2. [Color figure can be viewed in the online issue, which is available at wileyonlinelibrary.com.]

n (>1) rotations per one axial oscillation at low R, rigid rotation ($n = 1$) at intermediate R and $n < 1$ at high R. The rotation period gradually increases with R and approaches, at the upper-R boundary of a simple (one-wave) pattern domain, that of the 1D motion.

(iii) The critical radius for the existence of rotating fronts is smaller than this of oscillating fronts of the first mode.

(iv) The critical radii of the Mode 1 and the Mode 3 oscillating front solutions are related as the corresponding eigenvalues μ_{mn}. This suggests that higher modes can be realized in larger systems.

The pattern selection crucially depends on the choice of initial conditions (IC): In the present article, we choose as IC for 3D simulations a certain 1D solution with perturbed temperature distribution in the vicinity of the front position:

$$y_{3D}|_{t=0} = y_{1D}[1 + a\sin(\pi(z - Z_f + 2\Delta)/3\Delta)\varphi(r,\phi)],$$
$$z \in (Z_f - 2\Delta, Z_f + \Delta), \quad \Delta = 0.05Z_f,$$

where a is an amplitude of perturbations (0.05–0.2), while the φ (r, ϕ) function defines perturbations in the transversal plane. The patterned states were obtained only if the amplitude of perturbations exceeds a certain threshold value, otherwise the 3D system exhibits a 1D transversally-homogeneous solution. Similar results concerning the effect of IC on pattern formation in PBRs were obtained in previous studies using either a shallow reactor model[15,30] or a 2D ($r - z$) model.[13]

We cannot, unfortunately, formulate the universal recipe for the choice of IC. To simulate the oscillating (nonrotating) waves, we applied transversal perturbations in the form

$$\varphi_1(r,\phi) = \sin(0.5\pi r)\sin(\phi), \ \varphi_3(r,\phi) = \sin(0.5\pi r)$$

to the temperature field. These resemble the transversal eigenfunctions Eq. 2 for the first ($\mu_{11} = 1.84$) and the third ($\mu_{01} = 3.83$) modes, respectively. To simulate rotating 3D fronts, we produced the 2D cylindrical shell model simulations[12] first (rotating front branch was found with $R = 0.015 - 1.125$) yielding profiles $x(\xi, \theta)$, and $y(\xi, \theta)$. These profiles were imposed as IC at the external boundary ($r = 1$) of the 3D cylinder. The transversally averaged values $\bar{x}(\xi) = \langle x(\xi, \theta)\rangle$, $\bar{y}(\xi) = \langle y(\xi, \theta)\rangle$ were applied at the disk core ($0 < r < r_c \simeq 0.5$, we did not study the effect of r_c), whereas in the rest domain ($r_c < r < 1$) the IC were determined by interpolation between the core and the edge values. As soon as the rotating branch of the 3D problem was obtained, it was traced further by gradually increasing/decreasing R.

Note that in the present study we focus on the case of relatively small reactor radius around the bifurcation points. In this domain, the boundary conditions can induce a stabilizing effect. To check the effect of IC more carefully and to inquire which type of patterns can be induced by a small amplitude white noise, it is necessary to consider large domains, which is beyond the scope of the study.

The present study can be considered as numerical experiments showing coexistence of different types of transversal patterns in RDA systems. We aimed to detect simple (one-wave) types of transversal patterns rather then to construct full bifurcation diagrams of the sustained structures and to study their dynamic features using principal-component analysis. We expect to find also other transversal patterns that include: (i) spatially multiperiodic rotating pattern (similar to multi-wave patterns simulated with a cylindrical shell model[12]), (ii) outward moving patterns superimposed on the oscillating front (similar to the inward pattern shown in Figure 14), (iii) complex oscillating patterned fronts with different frequencies of axial and transversal oscillations (similar to mixed rotating–oscillating fronts), (iv) rich dynamics with frequency locked solutions and even chaos.

As 3D simulations involve significant efforts, 2D analogies should be helpful. The observation that the critical bifurcation radii of the Mode 1 and Mode 3 oscillating fronts are related as the corresponding transversal eigenvalues, suggests that transversal patterns formation in the form of eigenfunction (2) in the 3D case can be predicted by analysis of the reduced 2D cylindrical shell model. Relation (A1) (see Appendix) follows from the linear theory only close to the bifurcation point from a steady state, but we are not aware of a such general result.

Acknowledgments

This work is supported by Israel-US BSF. O.N. is partially supported by the Center for Absorption in Science, Ministry of Immigrant Absorption State of Israel. M.S. is a member of the Minerva Center of Nonlinear Dynamics and Complex Systems.

Literature Cited

1. Boreskov GK, Matros YuSh, Klenov OP, Logovkoi VI, Lakhmostov VS. Local nonuniformities in a catalyst bed. *Dokl Akad Nauk SSSR*. 1981;258:1418–1420.
2. Matros YuSh. *Unsteady Processes in Catalytic Reactors*. Amsterdam: Elsevier, 1985.
3. Barkelew CH, Gambhir BS. Stability of trickle-bed reactors. *ACS Symp Ser*. 1984;237:61–81.
4. Wicke E, Onken HU. Periodicity and chaos in a catalytic packed bed reactor for CO oxidation. *Chem Eng Sci*. 1988;43:2289–2294.
5. Wicke E, Onken HU. *Bifurcation, periodicity and chaos by thermal effects in heterogeneous catalysis*. In: Markus M, Muller SC, Nicolis G editors. *From Chemical to Biological Organization*. Berlin/New York: Springer-Verlag, 1988:68–81.
6. Marwaha B, Annamalai J, Luss D. Hot zone formation during carbon monoxide oxidation in a radial flow reactor. *Chem Eng Sci*. 2001;56:89–96.
7. Marwaha B, Luss D. Hot zone formation in packed bed reactors. *Chem Eng Sci*. 2003;58:733–738.
8. Digilov R, Nekhamkina O, Sheintuch M. Thermal imaging of breathing patterns during CO oxidation on a Pd/glass cloth. *AIChE J*. 2004;1:163–172.
9. Viswanathan GA, Sheintuch M, Luss D. Transversal hot zones formation in catalytic packed bed reactors. *Ind Eng Chem Res*. 2008; 47:7509–7523.
10. Froment G, Bischoff K. *Chemical Reactor Analysis and Design*. New York: Jonh Wiley and Sons, 1990.
11. Skadinskii KG, Khaikin BI, Merzhanov AG. Propagation of a pulsating exothermic reaction front in the condensed phase. *Fizika Gorenia i Vzruva*. (in Russian) 1971;7:19.
12. Sheintuch M, Nekhamkina O. Thermal patterns in simple models of cylindrical reactors. *Chem Eng Sci*. 2003;58:1441–1451.
13. Viswanathan GA, Luss D. Hot zones formation and dynamics in long adiabatic packed-bed reactors. *Ind Eng Chem Res*. 2006;45: 7057–7066.
14. Balakotaiah V, Gupta N, West DH. A simplified model for analyzing catalytic reactions in short monoliths. *Chem Eng Sci*. 2000;55: 5367–5383.

15. Viswanathan G, Bindal A, Khinast J, Luss D. Stationary transversal hot zones in adiabatic packed bed reactors. *AIChE J*. 2005;51:3028–3038.
16. Gupta A, Chakraborty S. Linear stability analysis of high- and low-dimensional models for describing mixing-limited pattern formation in homogeneous autocatalytic reactors. *Chem Eng J*. 2009;145:399–411.
17. Wicke E, Vortmeyer D. Zundzonen heterogener reactionen in gas-durchstromten Kornerschichten. *Bericht Bunsengesellschaft*. 1959; 63:145–152.
18. Kiselev OV. *Theoretical Study of the Phenomena of Heat Waves Movement in Catalytic Bed* (in Russian). Novosibirsk: Russian Academy of Sciences, Institute of Catalysis, 1993.
19. Nekhamkina O, Sheintuch M. Approximate characteristics of a moving temperature front in a fixed-bed catalytic reactor: effect of Pe_c. *Chem Eng J*. 2009;154:115–119.
20. Nekhamkina O, Sheintuch M. Transversal moving-front patterns. Criteria and simulations for two-bed and cylindrical shell packed-bed reactors. *Chem Eng Sci*. 2008;63:3716–3726.
21. Viswanathan GA, Luss D. Model prediction of hot spots formation in shallow adiabatic packed-bed reactors. *AIChE J*. 2006;52:1533–1538.
22. Horvath D, Petrov V, Scott SK, Showalter K. Instabilities in propagating reaction-diffusion fronts. *J Chem Phys.* 1993;98:6332–6342.
23. Malevanets A, Careta A, Kapral R. Biscale chaos in propagating fronts. *Phys Rev E*. 1995;52:4724–4735.
24. Toth A, Horvath D, Jakab E, Merkin JH, Scott SK. Lateral instabilities in cubic autocatalytic reaction fronts: the effect of autocatalyst decay. *J Chem Phys*. 2001;114:9947–9952.
25. Merkin JH, Kiss IZ. Dispersion curves in the diffusional instability of autocatalytic reaction fronts. *Phys Rev E*. 2005;72:026219.
26. Merkin JH. The effect of complexing agent on the transverse stability of autocatalytic reaction fronts. *J Chem Phys*. 2009;131:034506.
27. Balakotaiah V, Christaforatou EL, West DH. Transverse concentration and temperature non-uniformities in adiabatic packed bed catalytic reactors. *Chem Eng Sci*. 1999;54:1725–1734.
28. Agrawal R, West DH, Balakotaiah V. Modeling and analysis of local hot spot formation in down-flow adiabatic packed-bed reactors. *Chem Eng Sci*. 2007;62:4926–4943.
29. Viswanathan GA, Luss D. Moving transversal hot zones in adiabatic, shallow packed-bed reactors. *AIChE J*. 2006;52:705–717.
30. Sundarram S, Viswanathan G, Luss D. Reactor diameter impact on hot zone dynamics in an adiabatic packed bed reactor. *AIChE J*. 2007;53:1578–1590.
31. Winfree AT. *The Geometry of Biological Time*. Berlin: Springer, 2000.
32. Krinsky V, Swinney H, editors. *Wave and Patterns in Biological and Chemical Excitable Media*. North-Holland: Amsterdam, 1991.
33. Kapral R, Showalter K, editors. *Chemical Waves and Patterns*. Dordrecht: Kluwer, 1995.
34. Zykov VS. *Simulation of Wave Processes in Excitable Media*. Manchester: Manchester University Press, 1987.
35. Jahnke W, Skaggs WE, Winfree AT. Chemical vortex dynamics in the Belousov-Zhabotinsky reactor and in the two-variable Oregonator model. *J Chem Phys*. 1989;93:740–749.
36. Mikhailov AS. *Foundation of Synergetics I*. Springer-Verlag, 1994.
37. Zykov VS. Selection mechanism for rotating patterns in weakly excitable media. *Phys Rev E*. 2007;75:046203.
38. Sheintuch M, Nekhamkina O. Pattern formation in homogeneous reactor models. *AIChE J*. 1999;45:398–409.
39. Barto M, Sheintuch M. Excitable waves and spatiotemporal patterns in a fixed-bed reactor. *Am Inst Chem Eng J*. 1994;40:120–126.

Appendix

Consider an RDA system governed by a vector of state variables $\mathbf{U}$:

$$\mathbf{U}_t + V\nabla_z\mathbf{U} - \mathbf{D}\Delta_z\mathbf{U} - \mathbf{D}\Delta_\perp\mathbf{U} = \mathbf{G}(\mathbf{U})$$

As a first step, the basic 1D axial (z-dependent) solution is calculated which is frozen either in a laboratory, or in a moving coordinate system. At the second step, the linear stability analysis of the obtained solution is also conducted numerically with respect to perturbations ($\mathbf{u}$) of the form $\mathbf{u} \propto \Phi(z)e^{\lambda t}F_\perp$, where $\Phi(z)$ and $F_\perp$ the axial and the transversal eigenfunctions, respectively. The latter satisfy the same equation for both RDA and RD systems:

$$\Delta_\perp F_\perp + \mu^2 F_\perp = 0$$

where μ is the transversal eigenvalue.

Such an approach allows to determine in a 2D problem a continuous spectrum of the spatial wave number μ for an unbounded (in the transversal direction) planar domain and a critical shell (actually ring) radius corresponding to the first mode (R^1_{ring}) for the cylindrical shell model. The form of transversal eigenfunctions $\mathbf{F}_\perp$ depends on applied boundary conditions. In the case of no-flux BC at the external boundary $r = 1$ the corresponding functions are

$$F_\perp(r,\phi) = J_m(\mu_{\text{mn}}r)\exp(im\phi)$$

where the radial eigenfunctions $J_m(\mu_{\text{mn}}r)$ are the Bessel functions of the first kind. The discrete spectrum of the transversal eigenvalues μ_{mn} is defined by boundary conditions: $dJ_m(\mu_{\text{mn}}r)/dr|_{r=1} = 0$. Obviously, the transversal eigenfunctions in the $(r-\phi)$ plane of a 3D model (2) are exactly the same as those of a shallow reactor model on a disk. Note that the critical radius of the (mn) mode of a disk model ($R^{\text{mn}}_{\text{disk}}$) is related with the radius of the first mode in a 2D cylindrical shell model (R^1_{ring}) as

$$R^{\text{mn}}_{\text{disk}} = \mu_{\text{mn}}R^1_{\text{ring}} \tag{A1}$$

Manuscript received Oct. 19, 2009, and revision received Jan. 24, 2010.